IEEE Access
Multidisciplinary | Rapid Review | Open Access Journal

SPECIAL SECTION ON ADVANCED MODELING AND CONTROL OF COMPLEX MECHATRONIC SYSTEMS WITH NONLINEARITY AND UNCERTAINTY

Received January 2, 2018, accepted February 20, 2018, date of publication March 8, 2018, date of current version March 19, 2018.

Digital Object Identifier 10.1109/ACCESS.2018.2809608

Robust Predictive Current Control With Variable-Gain Adaptive Disturbance Observer for PMLSM

RUI YANG, (Student Member, IEEE), MING-YI WANG, LI-YI LI, (Member, IEEE), CHENG-MING ZHANG, AND JIA-LIN JIANG

Department of Electrical Engineering, Harbin Institute of Technology, Harbin 150001, China

Corresponding author: Li-Yi Li (liliyi.hit@gmail.com)

This work was supported in part by the State Key Program of National Natural Science of China under Grant 51537002, in part by the State Major Program of National Natural Science of China under Grant 51690182, in part by the National Natural Science of China Youth Fund under Grant 51707046, and in part by the National Natural Science of China under Grant 51677041.

ABSTRACT For high-velocity/high-precision linear motion systems, one of the most important factors that influence their dynamic performance is the characteristic of the inner current loop. The proportional–integral controller is the most practical strategy used for current control. However, its linear structure and imperfect decoupling capability make it difficult to obtain satisfying transient response under multiple operation conditions. The predictive current control (PCC) is designed as the current controller contributes to its superior performance. The main drawback of the PCC lies in its sensitivity against the unavoidable disturbances due to the parameters mismatch and the unmodeled dynamics. In this paper, an online adaptation-gain update method that can extend the inductance robust limit is proposed. First, by analyzing the closed-loop transfer function of the PCC system in the discrete domain, the effect of disturbances is discussed. Then, to eliminate the static current errors and improve the transient response, an adaptive disturbance observer is introduced. However, the direct dependence of the equivalent integral gain of the observer on the inductance in the controller leads to the deteriorative current response as the larger inductance mismatch exists. Therefore, an improved variable-gain method utilizing the current estimation errors is developed to reduce the current overshoot and the oscillation. Meanwhile, the design consideration for the two additional parameters of the proposed method is made by full-digital simulation. Finally, the effectiveness of the proposed method is uniformly verified with both simulation and experimental results.

INDEX TERMS Adaptive method, disturbance observer, permanent magnet linear synchronous machines (PMLSMs), predictive current control.

I. INTRODUCTION

As demand increases for high-velocity/high-precision linear motion systems, the PMLSMs have been widely applied to the precision applications [1], [2], such as the semiconductor manufacturing equipment, the computer numerical controlled (CNC) machine tools and the robotic systems, due to its significant advantages of high force density, rapid dynamic response and low thermal losses [3], [4]. Different with traditional rotary-type motors with reduction gears and ball screws, the thrust is exerted to the load directly without the mechanical transfer links in linear-driven motion systems [5]. Therefore, fast and accurate thrust output, namely, high-dynamic and high-precision current regulation is of great significance.

Contributing to the simple control schemes and its fast-dynamic response, the direct thrust control strategies combined with modern control methods have aroused wide attention recently [6]–[12], but the inherent relatively large force ripple limits its application in precision-area. Based on the above considerations, the current controller utilizing classical proportional-integral (PI) control [13] or predictive control can be proper candidate [14] at present. The good performance of zero steady-state current error and fixed switching frequency of the PI-controller has promoted its extensive industrial application. However, for the nonlinear, multivariable, and strong-coupled PMLSM control systems together with unavoidable external disturbances and internal parameter variations, satisfying transient response is difficult

to be obtained due to the linear control structure of the PI-controller and its imperfect decoupling capability [15], [16].

As model-based control method, the deadbeat predictive current control (PCC) can calculate the reference voltage for the next control instant directly with the discretized mathematical model. Compared with the finite-control-set model predictive current control [17], the switching frequency of the PCC [18] is constant and relatively higher, thus leading to lower current ripples. Therefore, the PCC is promising for the inner current loop design.

Ideally, the reference current can be tracked completely with a two-step delay with PCC. In reality, it is difficult to acquire the motor parameters accurately due to the measurement errors and their time-varying features under different operation conditions such as temperature rising and magnetic saturation [20], [21]. Therefore, the unavoidable parameters mismatch will exist between the controller and the actual plant and then the system performance and even its stability will be affected significantly. Based on this consideration, many works have been done to improve the robustness of PCC against parameters mismatch, and they can be roughly categorized into the following two aspects.

Most directly, the parameter identification methods can be utilized to update the parameters of PCC online. However, the simultaneous accurate estimation of all parameters (i.e., resistance, d- and q-axis inductance, and permanent magnet flux) of synchronous electrical machines is impossible due to the rank-deficient feature of d- and q-axis dynamic equations [22]. Therefore, many indirect identification or estimation methods were applied to enhance the performance of PCC. In [23], an adaptive parameter estimation scheme was proposed to estimate the three parameters iteratively. In [24], the integrals with d- and q-axis current errors were proposed to adjust the parameters online, then the static error current can be eliminated under the steady-state. However, the method neglected the effect of resistance and the transient performance was not analyzed yet.

Indirectly, the effect of parameters mismatch and unmodeled dynamics can be considered as lumped disturbances, and then the disturbance estimation/observation methods combined with the feedforward compensation can be utilized to promote the transient response and eliminate the static current error accordingly. In [25], a simple integral compensation with errors between the reference currents and the sampled one is added in parallel to the PCC. However, the selection of the integral-gain should be carefully balanced between the current response speed and its overshoot. With the development of modern control theories, varieties of methods have been expanded to improve the robustness of PCC. In [26] and [27], the linear Luenberger observer was designed to observe the effect of model uncertainties and the observer gains can be easily tuned with the pole-placement technique. Contributing to the invariant principle to external and internal disturbances of sliding mode, an improved reaching law-based sliding mode observer (SMO) [18] and the high-order SMO [28], [29] were designed to estimate the lumped disturbances with reduced chattering. Although the better observation and compensation effect can be obtained, the detailed instruction for the gain tuning remains to be studied. The extended Kalman filter (EKF) was designed to estimate the current of next sampling instant for the command voltage calculation of PCC [30]. The robustness against parameter variations makes the EKF a promising optimization method, however, the more calculation burden limits the sampling frequency. Considering the lumped disturbances as an extended state, the extended state observer (ESO) was also proposed to estimate the disturbances in [31].

An adaptive disturbance observer based on the model reference adaptive system was emerged in the PCC in [32]–[34], and then a simple adaptive law was deduced with the Lyapunov function. Then the disturbances were simply estimated by the integral with the current estimation errors between the output of the internal model and the actual plant. However, the equivalent integral-gains were inversely proportional to the inductances in the controller, and thus the large mismatch of inductances would cause large overshoot and even more oscillations. Therefore, a proportional term was added to the adaptive law in [35] to improve the estimation performance during the transient periods.

In high dynamic operation, serious magnetic saturation can be easily caused due to large current requirement and then large inductance deviation from the nominal one can be created. To enhance the robustness of PCC against inductance mismatch, a simple variable-gain method was proposed in the previous conference paper [36]. This paper will further address the stability proof, the detailed considerations for gain-tuning and sufficient experimental verification.

This paper is organized as follows. Section II introduces the PCC with disturbances compensation in discrete domain. Section III analyzes the basic process and the stability of the proposed variable-gain adaptive disturbance observer (VG-ADO). The method for gain-tuning and the compared simulation and experimental results with the constant-gain method (CG-ADO) proposed in [32]–[34] and the method in [35] are given in Section IV. Conclusions are summarized in Section V.

II. DISCRETE PCC SYSTEM

A. MODEL OF PMLSM

The dynamic model of the PMLSM in the synchronous d-q frame considering disturbances caused by parameters mismatch and unmodeled dynamics can be expressed as

$$\begin{cases} v_q = R_o i_q + L_{so}\dfrac{di_q}{dt} + \omega_e L_{so} i_d + \omega_e \lambda_{fo} + d_q \\ v_d = R_o i_d + L_{so}\dfrac{di_d}{dt} - \omega_e L_{so} i_q + d_d \end{cases} \tag{1}$$

where v_q, v_d are the applied q- and d-axes stator voltages; i_q, i_d, the q- and d-axes stator currents; L_s, the stator inductance of the surface-mounted PMLSM; R, the phase winding resistance; λ_f, the permanent magnet flux linkage; $\omega_e = v\pi/\tau$, in which v is the linear velocity of the mover and

τ is the pole-pitch, the subscript "o" denotes the nominal values and d_q, d_d represents lumped disturbances due to parameters mismatch and unmodeled dynamics, and they can be given by

$$\begin{cases} d_q = \Delta R i_q + \Delta L_s \dfrac{di_q}{dt} + \omega_e \Delta L_s i_d + \omega_e \Delta \lambda_f + \varepsilon_q \\ d_d = \Delta R i_d + \Delta L_s \dfrac{di_d}{dt} - \omega_e \Delta L_s i_q + \varepsilon_d \end{cases} \tag{2}$$

where $R = R_o + \Delta R$, $L_s = L_{so} + \Delta L_s$, $\lambda_f = \lambda_{fo} + \Delta\lambda_f$, and ε_q, ε_d represents the lumped unmodeled dynamics of q- and d-axis, respectively.

Considering the zero-order-hold feature of the inverter in real digital control system [23], the dynamics in (1) can be described in discrete-time form as

$$\begin{cases} v_q(k) = R_o i_q(k) + \dfrac{L_{so}}{T_s}[i_q(k+1) - i_q(k)] \\ \qquad + \omega_e(k)[L_{so} i_d(k) + \lambda_{fo}] + d_q(k) \\ v_d(k) = R_o i_d(k) + \dfrac{L_{so}}{T_s}[i_d(k+1) - i_d(k)] \\ \qquad - \omega_e(k) L_{so} i_q(k) + d_d(k) \end{cases} \tag{3}$$

where T_s is the sampling period and k is the discrete sampling instant. Then the current dynamic equations in matrix form can be expressed as

$$\mathbf{I}(k+1) = \mathbf{G}_0 \cdot \mathbf{I}(k) + \mathbf{H}_0 \cdot \{\mathbf{V}(k) - \boldsymbol{\lambda}(k) - \mathbf{D}(k)\} \tag{4}$$

in which

$$\mathbf{I}(k) = [\, i_q(k) \quad i_d(k) \,]^T, \quad \mathbf{V}(k) = [\, v_q(k) \quad v_d(k) \,]^T,$$
$$\boldsymbol{\lambda}(k) = \left[\, \lambda_{fo} \pi v(k) / \tau \quad 0 \,\right], \quad \mathbf{D}(k) = [\, d_q(k) \quad d_d(k) \,]^T,$$
$$\mathbf{G}_0 = \begin{bmatrix} 1 - T_s R_o / L_{so} & -T_s \pi v / \tau \\ T_s \pi v / \tau & 1 - T_s R_o / L_{so} \end{bmatrix},$$
$$\mathbf{H}_0 = \begin{bmatrix} T_s / L_{so} & 0 \\ 0 & T_s / L_{so} \end{bmatrix}.$$

B. DISCRETIZED PCC WITH DELAY COMPENSATION

Ideally, the current command at kth instant can be sensed at the $(k+1)$th instant neglecting the control delay caused by the A/D conversion and control algorithm execution. However, in real digital control system utilizing DSP, the control delay cannot be eliminated completely due to the relatively slow execution speed. Thus, the calculated voltage command can only be updated at the next sampling instant adopting symmetric SVPWM scheme. Therefore, in reality, there exists a two-sampling-periods delay between the starting time of the current control and the sensing time of resultant currents.

The control delay will produce large overshoot and more oscillations with the q-axis current command step-changed. Generally, the delay can be released with predicting the currents of the next instant in advance as proposed in [37], of which the known states and commands of kth instant can be used to estimate the currents of $(k+1)$th instant as

$$\hat{\mathbf{I}}(k+1) = \mathbf{G}_0 \cdot \mathbf{I}(k) + \mathbf{H}_0 \cdot \{\mathbf{V}^*(k) - \boldsymbol{\lambda}(k) - \hat{\mathbf{D}}(k)\} \tag{5}$$

where the subscript "^" and "$*$" denote the estimated states and the command values, respectively.

Hence, the command voltages of the $(k+1)$th instant can be calculated with the estimated currents in (5) as

$$\mathbf{V}^*(k+1) = \mathbf{H}_0^{-1}\{\mathbf{I}^*(k+2) - \mathbf{G}_0 \cdot \hat{\mathbf{I}}(k+1)\} + \boldsymbol{\lambda}(k+1) + \hat{\mathbf{D}}(k+1) \tag{6}$$

where the back-EMF λ(k + 1) can be supposed varying linearly between two adjacent sampling intervals due to the relatively slow mechanical dynamics compared with the current dynamics in general, thus the estimated values can be given by

$$\boldsymbol{\lambda}(k+1) \approx 2\boldsymbol{\lambda}(k) - \boldsymbol{\lambda}(k-1). \tag{7}$$

Thus, the command voltages of the $(k+1)$th instant can be calculated in the present interval and then applied to the motor in the next sampling instant $(k+1)$ with equations (5)–(7). As ignoring the disturbances, i.e., $\mathbf{D}(k) = 0$, the reference currents can be fully tracked with a two-sampling-periods delay, and it will be analyzed in the next subsection.

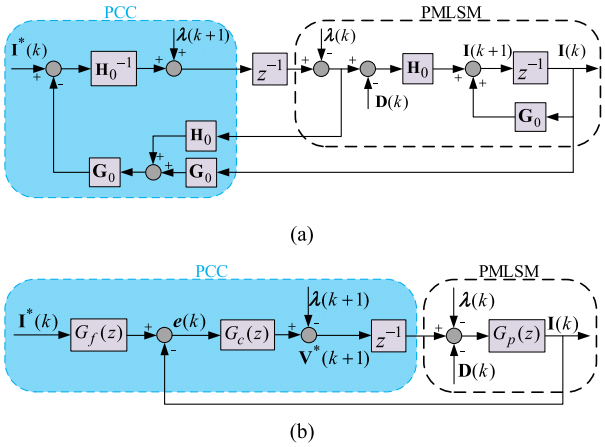

FIGURE 1. (a) Discrete control scheme of the conventional PCC and (b) the equivalent unit-feedback control diagram.

C. EFFECT OF DISTURBANCES

According to the above two parts, the overall discrete control scheme of PMLSM with PCC is depicted in Fig.1 (a). Considering the estimation of back-EMF in (7) as feedforward terms and noticing the control-delay effect, the back-EMF can be compensated effectively, i.e., $\lambda(k) \approx z^{-1}\lambda(k+1)$. Therefore, the equivalent unity-feedback control diagram can be deduced as shown in Fig.1 (b), in which the discrete transfer function of the feedback controller is

$$\mathbf{G}_c(z) = \mathbf{G}_0^2[\mathbf{I} + \mathbf{G}_0 z^{-1}]^{-1}\mathbf{H}_0^{-1} \tag{8}$$

and of the pre-filter is

$$\mathbf{G}_f(z) = \mathbf{G}_0^{-2}. \tag{9}$$

The discrete representation of the PMLSM is

$$\mathbf{G}_p(z) = \mathbf{H}_0[z\mathbf{I} - \mathbf{G}_0]^{-1}. \tag{10}$$

Then the transfer function matrix of the closed-loop control system can be described as

$$\mathbf{F}(z) = \mathbf{G}_f\mathbf{G}_c z^{-1}\mathbf{G}_p[\mathbf{I} + \mathbf{G}_c z^{-1}\mathbf{G}_p]^{-1} = z^{-2}\mathbf{I} \quad (11)$$

which indicates that the reference current can be fully tracked after two sampling periods neglecting the effect of disturbances due to parameter variations and unmodeled dynamics.

However, the disturbances exist inevitably in real system, i.e., $\mathbf{D}(k) \neq 0$. Then the current errors $\boldsymbol{e}(z)$ will be produced and the error transfer function to the disturbances can be deduced with zero reference from Fig.1 (b) as

$$\mathbf{F}_e(z) = \frac{\boldsymbol{e}(z)}{\boldsymbol{D}(z)} = \mathbf{G}_p[\mathbf{I} + \mathbf{G}_c z^{-1}\mathbf{G}_p]^{-1} \quad (12)$$

For simplicity, the step-changed disturbances with unity amplitude is considered here to evaluate its effect as follows

$$\boldsymbol{e}(\infty) = \lim_{z\to 1}\frac{z-1}{z}\mathbf{F}_e(z)\mathbf{D}(z) = \mathbf{H}_0[\mathbf{I} + \mathbf{G}_0] \quad (13)$$

where the disturbances are $\mathbf{D}(z) = (z-1)/z\mathbf{I}$. That is to say, the current errors will exist unless the disturbances can be eliminated accurately online.

For example, the disturbances caused by the resistance variation can be regarded as constant value because of they are coupled with the real currents, thus there will be steady-state current errors. Similarly, the variation of permanent magnet flux can also lead to steady-state current errors with nonzero velocity. In contrast, the effect of inductance variation is mainly coupled with the current change, so the transient performance will be largely affected in the current dynamic period while no static-current-errors will exist [18]. Therefore, the disturbance compensation methods must be configured to maintain the superior performance of PCC and that will be shown in next section.

III. VARIABLE-GAIN ADAPTIVE DISTURBANCE OBSERVER

Based on the model reference adaptive system, the lumped disturbances can be estimated with a simple adaptive law as shown in [32]–[34]. Then the feedforward compensation of estimated disturbances was utilized to alleviate or eliminate the effect of disturbances. However, the disturbance estimation dynamics with constant observer gain were largely deteriorated when large inductances mismatch exists. Hence, an improved variable-gain method is proposed in this section and the both methods will be presented here.

A. ADAPTIVE DISTURBANCE OBSERVER

To deduce the adaptation law for disturbance estimation, the dynamic equations described in continuous domain will be used in this subsection. Rearranging the cross-coupling terms to the side of control voltage, the equations (1) and (2) can be rearranged in state-equation form as

$$\begin{cases}\dot{\boldsymbol{x}} = \boldsymbol{A}_{co}\boldsymbol{x} + \boldsymbol{B}_{co}\boldsymbol{u} + \boldsymbol{G}_{co}\boldsymbol{d} \\ \boldsymbol{y} = \boldsymbol{C}\boldsymbol{x}\end{cases} \quad (14)$$

where

$$\boldsymbol{x} = [\,i_q \quad i_d\,]^T, \quad \boldsymbol{d} = [d_q \quad d_d]^T,$$
$$\boldsymbol{u} = [\,v_q - \omega_e L_{so} i_d - \omega_e \lambda_{fo} \quad v_d - \omega_e L_{so} i_q\,]^T,$$
$$\boldsymbol{A}_{co} = \begin{bmatrix} -R_o/L_{so} & 0 \\ 0 & -R_o/L_{so}\end{bmatrix}, \quad \boldsymbol{B}_{co} = \begin{bmatrix} 1/L_{so} & 0 \\ 0 & 1/L_{so}\end{bmatrix},$$
$$\boldsymbol{G}_{co} = \begin{bmatrix} -1/L_{so} & 0 \\ 0 & -1/L_{so}\end{bmatrix}, \quad \boldsymbol{C} = \begin{bmatrix} 1 & 0 \\ 0 & 1\end{bmatrix}.$$

For disturbance estimation, the reference model is selected as the internal model dynamics with nominal parameters. Then, the desired current response can be estimated with

$$\dot{\hat{\boldsymbol{x}}} = \boldsymbol{A}_{co}\hat{\boldsymbol{x}} + \mathbf{B}_{co}\boldsymbol{u} + \mathbf{G}_{co}\hat{\boldsymbol{d}}. \quad (15)$$

Subtracting (13) from (14), the error dynamics between the actual sampled currents and the estimated currents can be deduced as

$$\dot{\boldsymbol{e}} = \boldsymbol{A}_{co}\boldsymbol{e} + \boldsymbol{G}_{co}\tilde{\boldsymbol{d}} \quad (16)$$

where $\boldsymbol{e} = [e_{iq}\, e_{id}] = \boldsymbol{x} - \hat{\boldsymbol{x}}$ and $\tilde{\boldsymbol{d}} = \boldsymbol{d} - \hat{\boldsymbol{d}}$ denote estimation errors of the current and the disturbances, respectively.

To stabilize the error dynamics and ensure the estimation errors both converge to zero asymptotically, i.e., $\boldsymbol{e} = 0$ and $\tilde{\boldsymbol{d}} = 0$ as $t \to \infty$, the candidate Lyapunov function is selected as

$$V(\boldsymbol{e}(t), \tilde{\boldsymbol{d}}(t), t) = \frac{1}{2}\boldsymbol{e}^T(t)\boldsymbol{e}(t) + \frac{1}{2\gamma}\tilde{\boldsymbol{d}}^T(t)\tilde{\boldsymbol{d}}(t) \geq 0 \quad (17)$$

where γ is the adaptation gain to be designed.

Therefore, according to the Lyapunov stability theory, the time derivative of V must satisfy the following condition

$$\dot{V} = \boldsymbol{e}^T(t)\boldsymbol{A}_{co}\boldsymbol{e}(t) + \boldsymbol{e}^T(t)\boldsymbol{G}_{co}\tilde{\boldsymbol{d}} + \frac{1}{\gamma}\tilde{\boldsymbol{d}}^T(t)\dot{\tilde{\boldsymbol{d}}}(t) \leq 0. \quad (18)$$

Take note that the speed dynamics are much slower than the current dynamics, the variation of disturbances can be assumed slowly between two consecutive current sampling periods (equals to 200μs for 5kHz sampling frequency), i.e., $\dot{\boldsymbol{d}} \approx 0$. Then the adaptation law can be deduced with (18) as

$$\dot{\hat{\boldsymbol{d}}} = \gamma\mathbf{G}_{co}\boldsymbol{e}. \quad (19)$$

Therefore, the function $V(\boldsymbol{e}(t), \tilde{\boldsymbol{d}}(t), t)$ can be ensured bounded and nonincreasing due to $V(\boldsymbol{e}(0), \tilde{\boldsymbol{d}}(0), 0)$ is bounded. Then according to the Barbalat's Lemma [38], the errors of $\boldsymbol{e}(t)$ and $\tilde{\boldsymbol{d}}$ will converge to zero as $t \to \infty$.

As shown with (19), the disturbances can be simply estimated with the integral of the current estimation errors. The above adaptation law is easy to implement in real digital system. Meanwhile, the observer gain is the only parameter to be designed for balancing the observer bandwidth and the overshoot when nominal inductance is considered.

In reality, the inductance cannot be completely maintained in its nominal value due to the magnetic saturation especially when operating under high-dynamic condition. Therefore, the main drawback stands out as the equivalent integral-gain is also directly dependent on the inductance parameter

designed in the controller as described in the matrix $\boldsymbol{G}_{co}$. That is to say, the optimal performance or even the stability cannot be maintained when the actual motor inductance deviates largely from the nominal one, and this will be shown in Section IV.

An improved variable-gain method and the stable range of parameter γ will be discussed in the next subsection.

B. VARIABLE-GAIN ADAPTIVE DISTURBANCE OBSERVER

In order to reduce the effect of large inductances mismatch, the observer gain can be updated online utilizing the current estimation errors, and then a novel variable-gain adaptive method is proposed as

$$\begin{cases} \dot{\hat{\boldsymbol{d}}} = \chi \boldsymbol{G}_{co} \boldsymbol{e} \\ \chi = [\varepsilon + (1-\varepsilon) exp(-\delta \, |\boldsymbol{e}|)]\gamma \end{cases} \tag{20}$$

where $exp()$ denotes the exponential function, $\gamma > 0$ is the same as the value in (19), $\delta > 0$ and $0 < \varepsilon < 1$ are the two additional parameters to be designed.

The improved disturbance observation and thus better current dynamic response with (20) are discussed as following three aspects.

1) TRANSIENT-STATE PROCESS

It can be observed that if the absolute value of the estimation errors $|\boldsymbol{e}|$ is large enough, the variable χ approaches to the value $\varepsilon\gamma$ that is smaller than the value of γ in (19). This means that when the inductance is largely underestimated, i.e., the value in controller is smaller than the actual plant, the novel adaptation law has a comparative integral-gain or disturbance estimation speed compared with the constant-gain method in (19) under nominal parameters. Thus, large overshoot or oscillation caused by over-large integral-gain as the inductance is underestimated can be avoided, as will be shown in Fig.4. Meanwhile, as the inductance is overestimated, increased convergence time due to the smaller integral-gain can be balanced with smaller value of δ, thus a relatively larger gain approximating to γ can be obtained. In addition, large inductance and then large equivalent proportional-gain [37] can ensure superior transient response. Along with the estimation errors $|\boldsymbol{e}|$ decrease, the observer gain gradually increases.

2) STEADY-STATE PROCESS

On the other hand, as the errors $|\boldsymbol{e}|$ decrease to zero in steady-state, the variable χ converges to γ, thus the robustness against parameter variations can be ensured. Namely, the gain of the novel adaptive method can dynamically adapt to the variations of the estimation errors between $\varepsilon\gamma$ and γ, and then the dynamic performance of disturbances estimation due to the inductance mismatch can be improved while the steady-state current errors can be eliminated.

It should be pointed out here that the resistance and/or flux mismatch will also contribute to the errors $|\boldsymbol{e}|$, but the main part of $|\boldsymbol{e}|$ are caused by the inductance mismatch according to (2), especially in high-dynamic process. Meanwhile, compared with the method in (19), two additional parameters can be designed flexibly for desired dynamic response and immune steady-state accuracy. The detailed design considerations will be discussed in Section IV.

3) STABILITY

The stability of the novel adaptation law with nonlinear observer gain will be proved in this part. First, the discrete Lyapunov function is selected as

$$V(\boldsymbol{e}(k), k) = \frac{1}{2}\boldsymbol{e}(k)^T \boldsymbol{e}(k). \tag{21}$$

And then the convergence condition must be satisfied as

$$V(\boldsymbol{e}(k), k)[V(\boldsymbol{e}(k+1), k+1) - V(\boldsymbol{e}(k), k)] < 0. \tag{22}$$

The inequality equation (22) can be equivalent to (23) due to the condition $V(\boldsymbol{e}(k), k) > 0$ as follows:

$$V(\boldsymbol{e}(k+1), k+1) - V(\boldsymbol{e}(k), k) < 0. \tag{23}$$

For real digital implementation and stability analysis, the discretized form of (20) is expressed as

$$\hat{\mathbf{D}}(k+1) = \hat{\mathbf{D}}(k) - \chi(k)\mathbf{H}_0\boldsymbol{e}(k) \tag{24a}$$

$$\chi(k) = [\varepsilon + (1-\varepsilon) exp(-\delta \, |\boldsymbol{e}(k)|)]\gamma. \tag{24b}$$

Combine the equations (16), (21), (23) and (24), the stability range of the adaptation gain $\chi(k)$ is shown as

$$0 < \chi(k) < (2/h_0^2) \tag{25}$$

where $h_0 = T_s/L_{so}$ is related to the sampling period and the nominal inductance. Considering that the upper limit of variable χ is just the parameter γ, so the stable range of γ is same as (25).

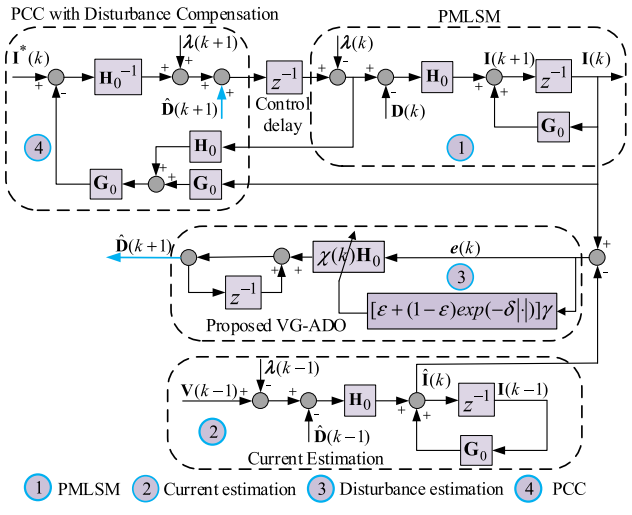

FIGURE 2. Discrete diagram of proposed VG-ADO based PCC.

The discrete diagram of the proposed VG-ADO based PCC system is shown in Fig.2, and the system consists of four main parts: the discrete PMLSM model, the proposed VG-ADO,

the current estimation and the PCC. The execution procedure of each part is numbered as depicted at the bottom of Fig.2, where the current estimation for the kth instant in step-2 is calculated one-sampling-period ahead with (5) as

$$\hat{\mathbf{I}}(k) = \mathbf{G}_0 \cdot \mathbf{I}(k-1) + \mathbf{H}_0 \cdot \{\mathbf{V}^*(k-1) - \boldsymbol{\lambda}(k-1) - \hat{\mathbf{D}}(k-1)\}. \quad (26)$$

Therefore, combining with (5), (6), (24) and (26), the proposed method can be easily implemented and the two main practical issues of PCC, namely, the effect of time-delay and the parameters mismatch [34], can be released. Moreover, the gain can be updated online with the current estimation errors, which will develop the disturbance estimation performance and thus maintain the current control capability of PCC.

TABLE 1. Main parameters of PMLSMs.

Parameters	Values	Unit
Nominal/Maximum thrust	600/1200	N
Nominal velocity	0.6	m/s
Stator resistance	6.5	Ω
Stator inductance	35	mH
Mover mass	45	kg
Thrust coefficient	94.2	N/A
Magnetic flux	0.24	Wb
Pole/Slot number	18/24	-

IV. SIMULATION AND EXPERIMENTAL RESULTS

Simulation and experimental tests are implemented to evaluate the effectiveness of the proposed method. The main parameters used in simulation are the same as the prototype motor under nominal conditions and are listed in Table I.

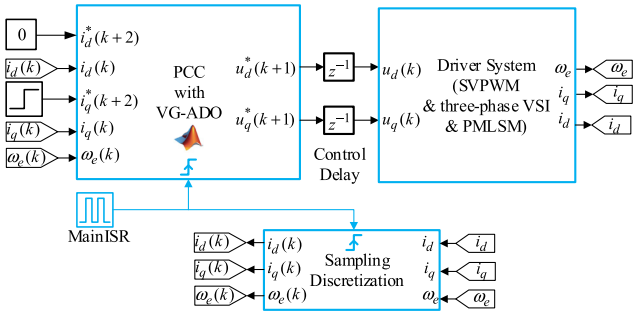

FIGURE 3. Discrete simulation model with MATLAB/Simulink.

A. SIMULATION RESULTS

In this subsection, the proposed method is simulated in the environment of MATLAB/Simulink with the same fully digital implementation procedure as the real control system. As depicted in Fig.3, the simulation model is composed of four main parts, i.e., the PCC, the driver system, the sampling discretization part and the control delay module. With the discrete simulation model, the response of real system can be mastered more effectively and the design of controller parameters can be obtained conveniently in advance. In the following part, the model is used to analyze the effect of the observer parameters on the current response and to further verify the effectiveness of the proposed method.

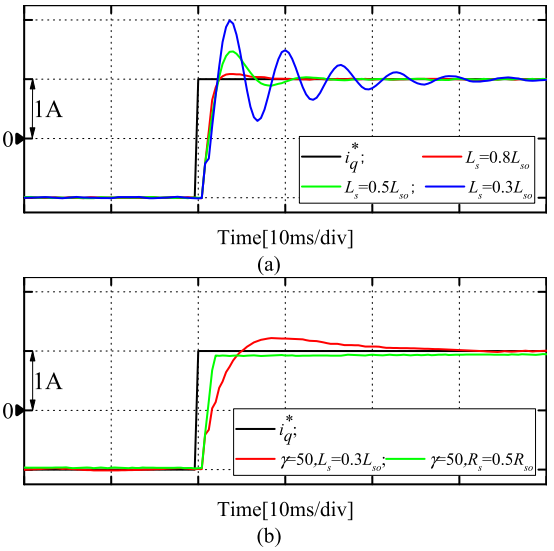

FIGURE 4. Simulated current step response with CG-ADO. (a) Different inductance mismatch with $\gamma = 1000$. (b) $L_s = 0.3L_{so}$ or $R_s = 0.5\,R_{so}$ with $\gamma = 50$.

1) CG-ADO BASED PCC

Firstly, the performance of the CG-ADO [32]–[34] was tested under different inductance mismatch. Fig.4 shows the dynamic q-axis current response as the reference steps up from −1[A] to 1[A]. The parameter γ is designed as 1000 for balance between the observer bandwidth and the current overshoot. It can be observed from Fig.4(a) that as the mismatch increases, larger overshoot and more oscillations occur in the current response, showing that the system approaches to the instability limit. That is to say, the robust range of inductance cannot be lower than $0.3L_{so}$ under $\gamma = 1000$.

As shown in Fig.4(b), decreasing the adaptation-gain γ can reduce the overshoot under $L_s = 0.3L_{so}$, while the smaller value of γ (such as 50) has to be designed to obtain approximate response with the proposed VG-ADO method as will be shown in Fig.5. However, the over-small integral-gain will lead to slow convergence speed as resistance and/or flux mismatch also exists in general. The green line in Fig.4(b) shows the current response with only resistance mismatch $R_s = 0.5R_{so}$ under $\gamma = 50$, it is obvious that the transient error exists more than 40[ms]. Therefore, the fast-convergence and small-overshoot disturbance estimation performance of CG-ADO cannot be still realized with underestimated inductance.

2) VG-ADO BASED PCC

To obtain both higher bandwidth and smaller overshoot with VG-ADO, the effect of observer parameters (ε and δ) on

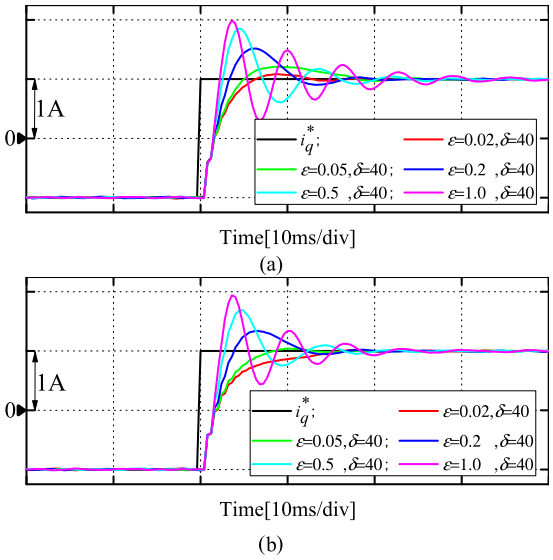

FIGURE 5. Simulated current step response with different gains of ε. (a) Under inductance mismatch ($L_S = 0.3L_{SO}$). (b) Under mismatch ($R_S = 0.5\,R_{SO}$, $L_S = 0.3L_{SO}$).

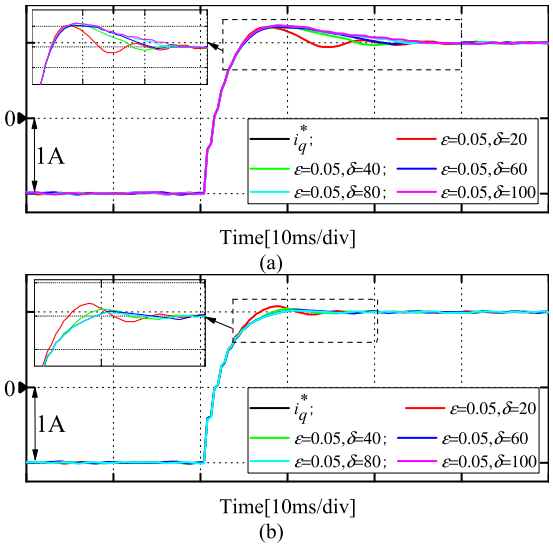

FIGURE 6. Simulated step current response with different gains of ε. (a) Under inductance mismatch ($L_S = 0.3L_{SO}$). (b) Under mismatch ($R_S = 0.5R_{SO}$, $L_S = 0.3L_{SO}$).

TABLE 2. Current response performance index under mismatch.

Performance Index	ε=0.02	ε=0.05	δ=40 ε=0.2	ε=0.5	ε=1.0
	Parameters mismatch: (L_s=0.3L_{so})/ (R_s=0.5R_{so}, L_s=0.3L_{so})				
Oscillation	4/1	4/2	4/3	6/5	16/14
Overshoot/A	0.08/0.02	0.21/0.04	0.5/0.34	0.85/0.7	1.0/0.94
Settling/ms	12/10	12/8	11/12	14/14	25/25

the transient response with mismatch is tested in simulation firstly. As depicted in Fig.5(a), maintaining the parameter $\delta = 40$ fixed, the overshoot and oscillations get smaller as the parameter ε decreases with inductance mismatch ($L_s = 0.3L_{so}$), while the settling time is approximately the same as the parameter ε is small as listed in Table II. That is because the smaller ε can lead to smaller or more suitable equivalent integral-gains compared with the CG-ADO method, as shown in (20) or (24a), so the disturbance caused by the inductance mismatch can be estimated more accurately. However, when considering the resistance variations, the over-small parameter ε (such as 0.02) will lead to slow convergence speed as illustrated in Fig.5(b). Thus, $\varepsilon = 0.05$ is selected for proper overshoot and convergence time as the resistance and inductance mismatch both exist in real system. Additionally, it can be noted that the CG-ADO is just the special case of the VG-ADO with $\varepsilon = 1.0$ and/or $\delta = 0$.

With the same method, the effect of parameter δ is also tested in simulation, as shown in Fig.6(a) and (b). It can be seen that the approximately same overshoot and convergence speed is obtained with inductance deviation only. As the inductance is underestimated, the larger current estimation errors will be caused, so the exponential term in (24) will converge to zero rapidly as long as the parameter δ is large enough. However, there exist more oscillations under smaller parameter $\delta = 20$ as illustrated in Fig.6(a). It can be explained that the VG-ADO approaches to the CG-ADO with smaller parameter δ. Fig.6(b) shows the current response with both resistance and inductance variations, which indicates that a little bigger overshoot exists with $\delta = 20$. Although larger parameter δ can reduce the overshoot, the value of $\delta = 40$ is chosen due to the current sampling noises can increase the varying range of adaptation-gain χ and thus deteriorate the steady-state robustness against disturbances. Therefore, the observer parameters can be properly designed as $\varepsilon = 0.05$ and $\delta = 40$.

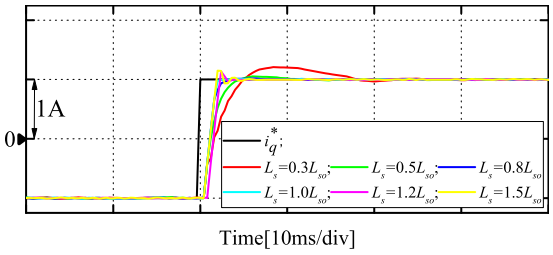

FIGURE 7. Simulated step current response with $\varepsilon = 0.05$ and $\delta = 40$ under different inductance mismatch.

Compared with the CG-ADO in Fig.4, better transient response with smaller overshoot and no oscillation is obtained under different inductance mismatch as shown in Fig.7, while the inductance ranges from $0.3L_{so}$ to $1.5L_{so}$. Meanwhile, the current response with nominal value is not affected any more.

To further verify the effectiveness of the VG-ADO, the flux variation is also added to the controller and it can be observed from Fig.8(a) that negligible overshoot of the q-axis current and the sinusoidal current of phase-A is obtained with

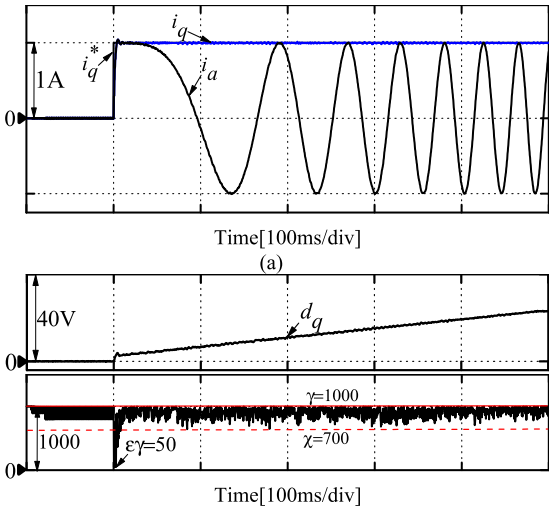

FIGURE 8. Simulated step current response with mismatch $R_s = 0.5R_{so}$, $L_s = 0.3L_{so}$ and $\lambda_f = 0.5\lambda_{fo}$ under VG-ADO.

zero-static-error. Fig.8(b) shows the estimated q-axes disturbances and the corresponding adaptation-gain. The constant slope of estimated disturbances in steady-state due to the flux deviation and the constant acceleration indicates the validity of the algorithm. It can be noted that the adaptation-gain decreases to the value $\varepsilon\gamma = 50$ simultaneously as the reference current steps up and maintains constant until the estimated current error being small enough, and then it converges to the value $\gamma = 1000$ gradually. Ideally, the adaptation-gain is equal to the parameter γ in steady-state, but it ranges from 700 to 1000 which is caused by the discretization of the adaptation law. Nevertheless, the robustness still can be maintained with underestimated inductance in steady-state. Although the small integral-gain leads to slower observer convergence speed as inductance is overestimated, the larger equivalent proportional-gain [37] with equation (3) can also preserve the performance fast current response.

The effect of the two additional parameters on the current response performance can be summarized as follows.

Remark 1: The performance of the current response is mainly dependent on the design of parameter ε which should be chosen carefully for both faster convergence speed and smaller overshoot. The smaller the parameter ε, the smaller current overshoot will be obtained, but the convergence speed will also be slower. In addition, decreasing the parameter ε, the inductance robust limit can be extended further.

Remark 2: In contrast, with proper design of ε, the effect of parameter δ is not very decisive. The smaller parameter δ can help to promote the noise rejection capability and the bigger one can speed up convergence.

In addition, the method in [35] was also designed and simulated here for comparation. The meaning of the parameter k_2 in [35] is the same as the gain γ, so it is designed as 1000 for fair evaluation. Considering the observer stability and the transient performance, the parameter k_1 is selected as 25. It can be observed from Fig.9 that the both methods

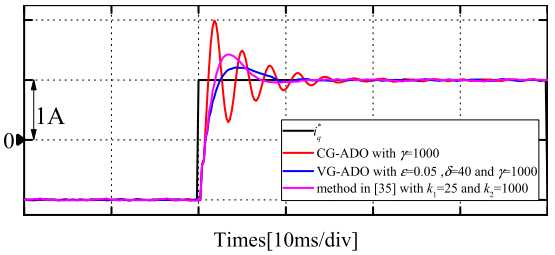

FIGURE 9. Simulated step current response with different methods under inductance variation ($L_s = 0.3L_{so}$).

can improve the dynamic performance of the current step response as the inductance is underestimated ($L_s = 0.3L_{so}$), but there exists larger overshoot and more oscillations in the method introduced in [35]. Therefore, the VG-ADO method is more superior than the method in [35]. The simulations of overestimated inductance and both with resistance and/or flux mismatch are not listed here for limited page.

Therefore, according to the simulation results, the proposed VG-ADO can develop the transient response and extend the robust limit of inductance compared with the methods in [32]–[35].

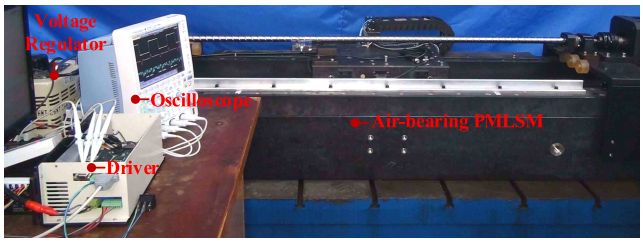

FIGURE 10. Experimental system.

B. EXPERIMENTAL RESULTS

To further verify the validity of the proposed method, an air-bearing test platform was built and the experimental system is depicted in Fig.10. The motor was driven with a full digital power amplifier based on the 32-bit floating-point DSP TMS320F28335 with 150MHz operation frequency. The amplifier adopted a three phase VSI with three sets of insulated-gate-bipolar-transistors (IGBTs) under the bus voltage of 100[V], which is converted from a-single-phase rectifier with a voltage regulator. The switching frequency was 5[kHz]. The currents of phase-windings were measured through two LEM current sensors with the nominal current of 25[A] and high accuracy of ±0.2%. For eliminating the effect of commutation spikes, the synchronous sampling technique with symmetric SVPWM was configured. The internal 12-bit A/D converter in the DSP processor was utilized. To reduce the noises of sampled current, the repeated sampling handling in software algorithm and the second-order Butterworth low-pass-filter in hardware circuits design were both used. The interested variables were displayed on the digital oscilloscope via an on-board 12-bit D/A converter with four channels

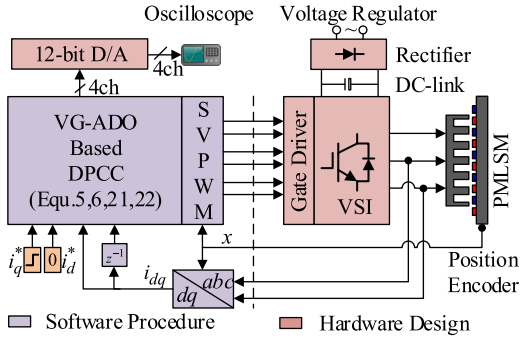

FIGURE 11. Block diagram of the experimental system.

and the updating-frequency was also 5[kHz]. The current of phase-A was directly measured with the current clamp. The simplified block diagram of the overall system is shown in Fig.11.

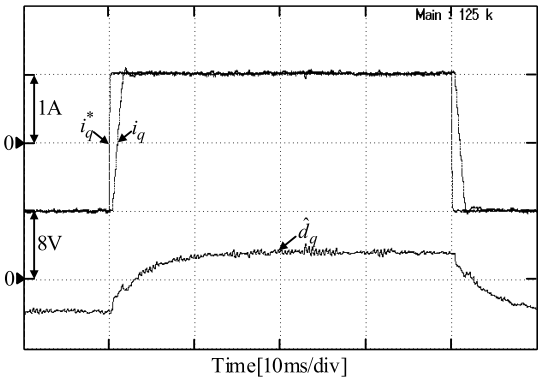

FIGURE 12. Tested square-wave current response with resistance mismatch ($R_s = 0.5R_{so}$) under CG-ADO.

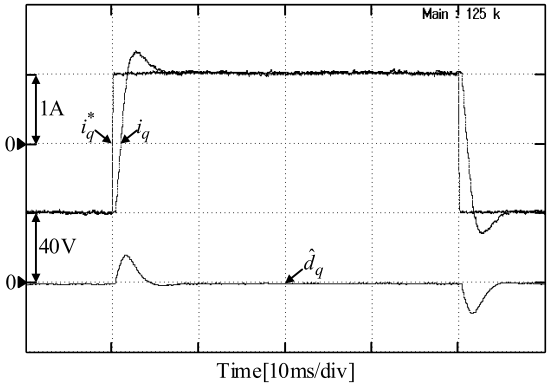

FIGURE 13. Tested square-wave current response with inductance mismatch ($L_s = 0.5L_{so}$) under CG-ADO.

1) CG-ADO BASED PCC

Firstly, as shown in Figs.12 and 13, the square-wave current response of PCC was tested with resistance mismatch ($R_s = 0.5R_{so}$) and inductance mismatch ($L_s = 0.5L_{so}$) under

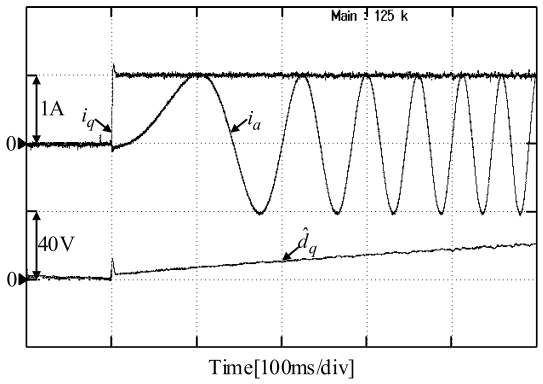

FIGURE 14. Tested step current response with mismatch ($R_s = 0.5R_{so}$, $L_s = 0.5L_{so}$ and $\lambda_f = 0.5\lambda_{fo}$) under CG-ADO.

CG-ADO respectively. The convergence time of the disturbance estimation is 10[ms] under resistance variation and the overshoot is 0.25[A] under inductance variation, which agrees well with the simulated one in Table II. In this paper, $\gamma = 1000$ was chosen to design the CG-ADO for balancing the convergence speed and the current overshoot. As the mismatch ($R_s = 0.5R_{so}$, $L_s = 0.5L_{so}$ and $\lambda_f = 0.5\lambda_{fo}$) exists, the small current overshoot, quick response and accurate disturbance estimation was obtained as shown in Fig.14 under step current command. Therefore, the effectiveness of the PCC with CG-ADO was verified.

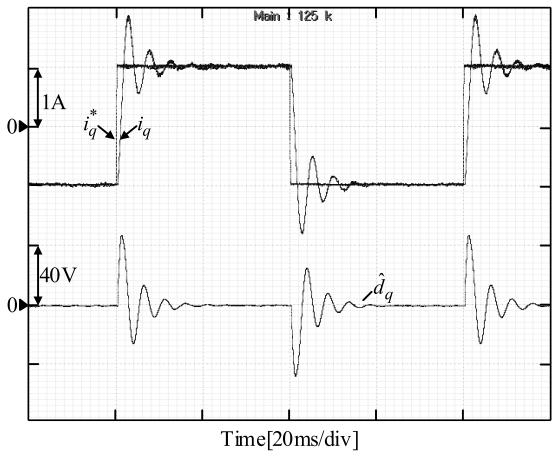

FIGURE 15. Tested square-wave current response with inductance mismatch ($L_s = 0.3L_{so}$) under CG-ADO.

However, as the inductance mismatch further increases to $L_s = 0.3L_{so}$, the large overshoot and more oscillations appear as depicted in Fig.15. The actual current response and the estimated one based on the internal model dynamics are shown in Fig.16. The large error as shown at the bottom of Fig.16 combined with the overlarge integral-gain contribute to the oscillating disturbance estimation with large overshoot (50[V]), which approaches to the inverter output limit (57.7[V] with the DC-bus voltage of 100[V]) as shown in Fig.15. Therefore, the superior performance of PCC under

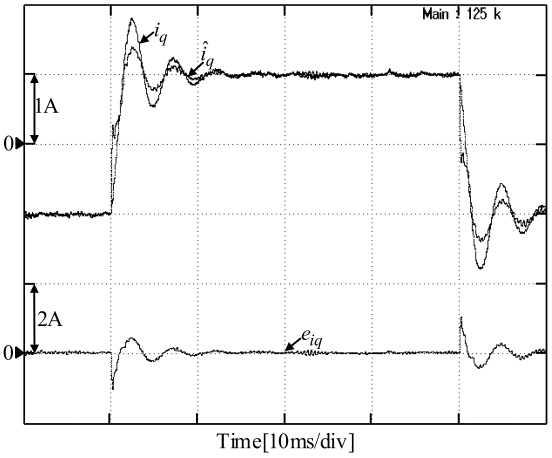

FIGURE 16. Estimated q-axis current and actual q-axis square-wave current response with inductance mismatch ($L_s = 0.3L_{so}$) under CG-ADO.

nominal parameters cannot be maintained with large inductance mismatch.

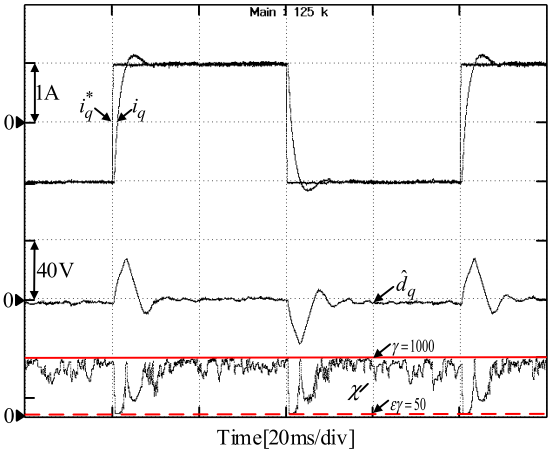

FIGURE 17. Tested square-wave current response with inductance mismatch ($L_s = 0.3L_{so}$) under VG-ADO.

2) VG-ADO BASED PCC

The estimated current errors were utilized here to regulate the adaptation-gain dynamically, and the square-wave current response of PCC with VG-ADO is illustrated in Fig.17 as only the inductance mismatch ($L_s = 0.5L_{so}$) exists. In real test, the parameter $\delta = 20$ is adjusted for reducing the varying range of adaptation-gain for considering the effect of current sampling noises and the ignored inverter nonlinearity, while the parameter $\varepsilon = 0.05$ remains unchanged. It is obvious that the large overshoot and more oscillations of the estimated disturbances and the current oscillations were eliminated.

The adaptation-gain was not constant but varied with the current state as shown in Fig.18. At the initial moment of the current reference, the estimated current error was large due to the overlarge deviation between the desired voltage command and the actual calculated one. Then, the adaptation-gain

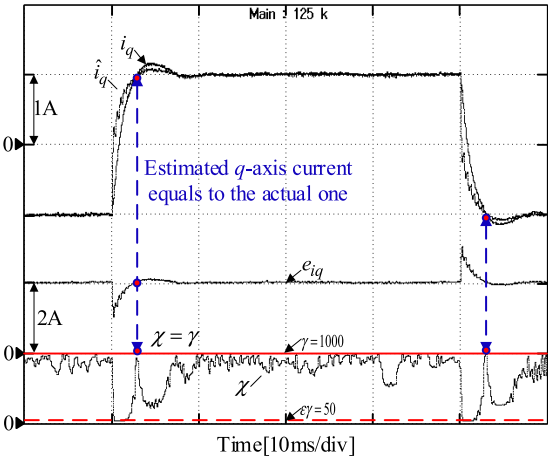

FIGURE 18. Estimated q-axis current and actual q-axis current square-wave response with inductance mismatch ($L_s = 0.3L_{so}$) under VG-ADO.

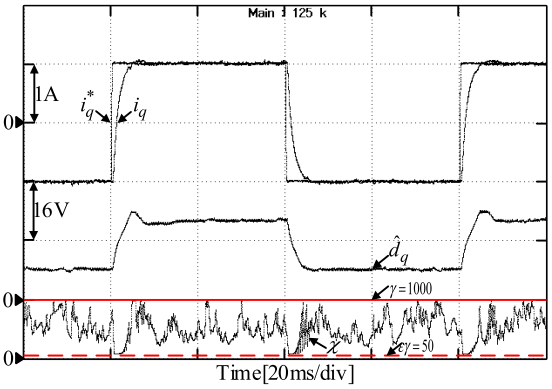

FIGURE 19. Tested square-wave current response with mismatch $R_s = 0.5R_{so}$ and $L_s = 0.3L_{so}$ under VG-ADO.

approaches to the smaller value of $\varepsilon\gamma = 50$. Thus, the underestimated inductance and the smaller adaptation-gain lead to reasonable integral-gain of the disturbance observer, which contributes to more proper disturbance compensation and then smaller current overshoot. As the estimated current equals to the actual sampled one, the gain χ turns to be $\gamma = 1000$ as the blue-dashed line shows. As approaching the steady-state, the errors get smaller and then the gain approaches to $\gamma = 1000$. The variation of the gain was caused by the current sampling noises, nevertheless, the robustness can still be ensured as the varying range is small.

The current response under VG-ADO with mismatch ($R_s = 0.5R_{so}$ and $L_s = 0.3L_{so}$) is illustrated in Fig.19, and the results are approximately consistent with the simulated one in Fig.5(b) with green line. In addition, compared with the simulated results in Fig.9, the uniform response with slightly-different gain variation as shown in Fig.20 also proves the effectiveness of the proposed variable-gain adaptation law.

To further evaluate the performance of the VG-ADO, the condition of overestimated inductance was also tested as shown in Fig.21. It can be observed that the transient response

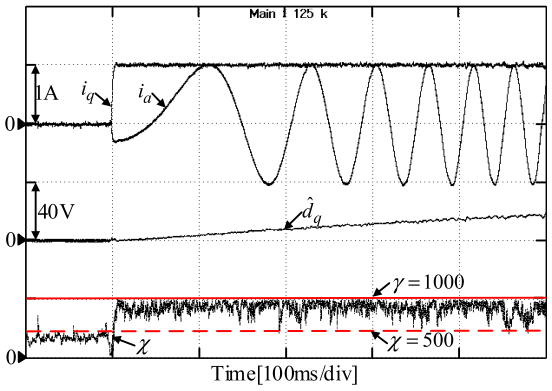

FIGURE 20. Tested step current response with mismatch $R_s = 0.5R_{so}$, $L_s = 0.3L_{so}$ and $\lambda_f = 0.5\lambda_{fo}$ under VG-ADO.

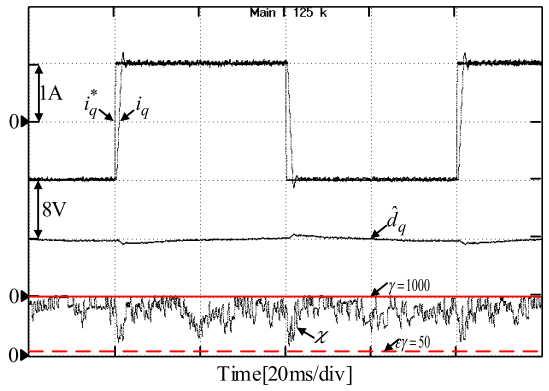

FIGURE 21. Tested square-wave current response with mismatch $L_s = 1.5L_{so}$ under VG-ADO.

was not affected. Therefore, when the inductance varies between $0.3L_{so}$ and $1.5L_{so}$, the better transient response of PCC and zero-static-error characteristic can still be maintained with the proposed method.

In summary, the effectiveness of the proposed VG-ADO based PCC was both verified by the simulation and experimental results.

V. CONCLUSIONS

In this paper, an improved variable-gain adaptive disturbance observer for extending the inductance robustness is described. The disturbance observer is designed with the model reference adaptive system and the observer gain is updated online dynamically by utilizing the current estimation errors. The full-digital simulation is used to discuss the effect of the two additional parameters on the transient current response. The large overshoot and more oscillations of the current response when using the constant-gain method are reduced/eliminated with the proposed method. Thus, the robust inductance range has been extended effectively. And both the simulation and experimental results verify its effectiveness. In future work, the more detailed analyzation of the inductance robust range with respect to the observer parameters will be studied.

REFERENCES

[1] K. Cho, J. Kim, S. B. Choi, and S. Oh, "A high-precision motion control based on a periodic adaptive disturbance observer in a PMLSM," *IEEE/ASME Trans. Mechatronics*, vol. 20, no. 5, pp. 2158–2171, Oct. 2015.

[2] K. K. Tan, H. Dou, Y. Chen, and T. H. Lee, "High precision linear motor control via relay-tuning and iterative learning based on zero-phase filtering," *IEEE Control Syst. Technol.*, vol. 9, no. 2, pp. 244–253, Mar. 2011.

[3] F. J. Lin, J. C. Hwang, P. H. Chou, and Y. C. Hung, "FPGA-based intelligent-complementary sliding-mode control for PMLSM servo-drive system," *IEEE Trans. Power Electron.*, vol. 25, no. 10, pp. 2573–2587, Oct. 2010.

[4] C.-H. Ting and Y.-N. Chang, "Observer-based backstepping control of linear stepping motor," *Control Eng. Pract.*, vol. 21, no. 7, pp. 930–939, Jul. 2013.

[5] K. Y. Lian, C. Y. Hung, C. S. Chiu, and L. C. Fu, "Robust adaptive control of linear induction motors with unknown end-effect and secondary resistance," *IEEE Trans. Energy Convers.*, vol. 23, no. 2, pp. 412–422, Jun. 2008.

[6] C.-C. Sung and Y.-S. Huang, "Based on direct thrust control for linear motor control systems," *IEEE Trans. Ind. Electron.*, vol. 56, no. 5, pp. 1629–1639, May 2009.

[7] Y. S. Huang and C. C. Sung, "Function-based controller for linear motor control systems," *IEEE Trans. Ind. Electron.*, vol. 57, no. 3, pp. 1096–1105, Mar. 2010.

[8] H. Karimi, S. V.-Zadeh., and F. R. Salmasi, "Combined vector and direct thrust control of linear induction motors with end effect compensation," *IEEE Trans. Energy Convers.*, vol. 31, no. 1, pp. 196–205, Oct. 2015.

[9] M. A. M. Cheema, J. E. Fletcher, D. Xiao, and M. F. Rahman, "A linear quadratic regulator-based optimal direct thrust force control of linear permanent-magnet synchronous motor," *IEEE Trans. Ind. Electron.*, vol. 63, no. 5, pp. 2722–2733, May 2016.

[10] M. A. M. Cheema, J. E. Fletcher, D. Xiao, and M. F. Rahman, "A direct thrust control scheme for linear permanent magnet synchronous motor based on online duty ratio control," *IEEE Trans. Power. Electron.*, vol. 31, no. 6, pp. 4416–4428, Jun. 2016.

[11] M. A. M. Cheema, J. E. Fletcher, M. F. Rahman, and D. Xiao, "Optimal, combined speed, and direct thrust control of linear permanent magnet synchronous motors," *IEEE Trans. Energy Convers.*, vol. 31, no. 3, pp. 947–958, Sep. 2016.

[12] M. A. M. Cheema, J. E. Fletcher, M. Farshadnia, D. Xiao, and M. F. Rahman, "Combined speed and direct thrust force control of linear permanent-magnet synchronous motors with sensorless speed estimation using a sliding-mode control with integral action," *IEEE Trans. Ind. Electron.*, vol. 64, no. 5, pp. 3489–3501, Jan. 2017.

[13] M. P. Kazmierkowski and L. Malesani, "Current control techniques for three-phase voltage-source PWM converters: A survey," *IEEE Trans. Ind. Electron.*, vol. 45, no. 5, pp. 691–703, Oct. 1998.

[14] P. Cortés, M. P. Kazmierkowski, R. M. Kennel, D. E. Quevedo, and J. Rodríguez, "Predictive control in power electronics and drives," *IEEE Trans. Ind. Electron.*, vol. 55, no. 12, pp. 4312–4324, Dec. 2008.

[15] L. Harnefors and H.-P. Nee, "Model-based current control of AC machines using the internal model control method," *IEEE Trans. Ind. Appl.*, vol. 34, no. 1, pp. 133–141, Jan./Feb. 1998.

[16] S. Li and Z. Liu, "Adaptive speed control for permanent-magnet synchronous motor system with variations of load inertia," *IEEE Trans. Ind. Electron.*, vol. 56, no. 8, pp. 3050–3059, Aug. 2009.

[17] H. A. Young, M. A. Perez, and J. Rodriguez, "Analysis of finite-control-set model predictive current control with model parameter mismatch in a three-phase inverter," *IEEE Trans. Ind. Electron.*, vol. 63, no. 5, pp. 3100–3107, May 2016.

[18] X. Zhang, B. Hou, and Y. Mei, "Deadbeat predictive current control of permanent-magnet synchronous motors with stator current and disturbance observer," *IEEE Trans. Power Electron.*, vol. 32, no. 5, pp. 3818–3834, May 2017.

[19] M. Siami, D. A. Khaburi, and J. Rodriguez, "Simplified finite control set-model predictive control for matrix converter-fed PMSM drives," *IEEE Trans. Power. Electron.*, vol. 33, no. 3, pp. 2438–2446, Mar. 2018.

[20] T. Sebastian, "Temperature effects on torque production and efficiency of PM motors using NdFeB magnets," *IEEE Trans. Ind. Appl.*, vol. 31, no. 2, pp. 353–357, Mar./Apr. 1995.
[21] K. J. Meessen, P. Thelin, J. Soulard, and E. A. Lomonova, "Inductance calculations of permanent-magnet synchronous machines including flux change and self- and cross-saturations," *IEEE Trans. Magn.*, vol. 44, no. 10, pp. 2324–2331, Oct. 2008.
[22] D. Q. Dang, M. S. Rafaq, H. H. Choi, and J.-W. Jung, "Online parameter estimation technique for adaptive control applications of interior PM synchronous motor drives," *IEEE Trans. Ind. Electron.*, vol. 63, no. 3, pp. 1438–1449, Mar. 2016.
[23] Y. A.-R. I. Mohamed and E. F. El-Saadany, "An improved deadbeat current control scheme with a novel adaptive self-tuning load model for a three-phase PWM voltage-source inverter," *IEEE Trans. Ind. Electron.*, vol. 54, no. 2, pp. 747–759, Apr. 2007.
[24] X.-H. Jin, Y. Zhang, and D.-G. Xu, "Static current error elimination algorithm for induction motor predictive current control," *IEEE Access*, vol. 5, pp. 15209–15250, 2017.
[25] H. Le-Huy, K. Slimani, and P. Viarouge, "Analysis and implementation of a real-time predictive current controller for permanent-magnet synchronous servo drives," *IEEE Trans. Ind. Electron.*, vol. 41, no. 1, pp. 110–117, Feb. 1994.
[26] K.-H. Kim, I.-C. Baik, G.-W. Moon, and M.-J. Youn, "A current control for a permanent magnet synchronous motor with a simple disturbance estimation scheme," *IEEE Trans. Control Syst. Technol.*, vol. 7, no. 5, pp. 630–633, Sep. 1999.
[27] B. Wang, X. Chen, Y. Yu, G. Wang, and D. Xu, "Robust predictive current control with online disturbance estimation for induction machine drives," *IEEE Trans. Power Electron.*, vol. 32, no. 6, pp. 4663–4674, Jun. 2017.
[28] B. Wang, Y. Yu, G. Wang, and D. Xu, "Static-errorless deadbeat predictive current control using second-order sliding-mode disturbance observer for induction machine drives," *IEEE Trans. Power Electron.*, vol. 33, no. 3, pp. 2395–2403, Mar. 2018.
[29] Y. Jiang, W. Xu, C. Mu, and Y. Liu, "Improved deadbeat predictive current control combined sliding mode strategy for PMSM drive system," *IEEE Trans. Veh. Technol.*, vol. 67, no. 1, pp. 251–263, Jan. 2018.
[30] M. Abdelrahem, C. Hackl, Z. Zhang, and R. Kennel, "Robust predictive control for direct-driven surface-mounted permanent-magnet synchronous generators without mechanical sensors," *IEEE Trans. Energy Convers.*, vol. 33, no. 1, pp. 179–189, Mar. 2018.
[31] M. Yang, X. Lang, J. Long, and D. Xu, "A flux immunity robust predictive current control with incremental model and extended state observer for PMSM drive," *IEEE Trans. Power Electron.*, vol. 32, no. 12, pp. 9267–9279, Dec. 2017.
[32] Y. A.-R. I. Mohamed, "Design and implementation of a robust current-control scheme for a PMSM vector drive with s simple adaptive disturbance observer," *IEEE Trans. Ind. Electron.*, vol. 54, no. 4, pp. 1981–1988, Aug. 2007.
[33] Y. A.-R. I. Mohamed and E. F. El-Saadany, "Robust high bandwidth discrete-time predictive current control with predictive internal model—A unified approach for voltage-source PWM converters," *IEEE Trans. Power Electron.*, vol. 23, no. 1, pp. 126–136, Jan. 2008.
[34] Y. A.-R. I. Mohamed and E. F. El-Saadany, "A current control scheme with an adaptive internal model for torque ripple minimization and robust current regulation in PMSM drive system," *IEEE Trans. Energy Convers.*, vol. 23, no. 1, pp. 92–100, Mar. 2008.
[35] K. H. Kim, "Model reference adaptive control-based adaptive current control scheme of a PM synchronous motor with an improved servo performance," *IET Electr. Power Appl.*, vol. 3, no. 1, pp. 8–18, Jan. 2009.
[36] R. Yang, M. Wang, C. Zhang, and L. Li, "Robustness improvement of predictive current control for PMLSM integrating adaptive internal model with time delay compensation," in *Proc. ICEMS*, 2017, pp. 1–5.
[37] H.-T. Moon, H.-S. Kim, and M.-J. Youn, "A discrete-time predictive current control for PMSM," *IEEE Trans. Power Electron.*, vol. 18, no. 1, pp. 464–472, Jan. 2003.
[38] K. J. Astrom and B. Wittenmark, *Adaptive Control*. Reading, MA, USA: Addison-Wesley, 1995.

RUI YANG (S'16) was born in Hubei province, China. He received the B.E. degree in electrical engineering from the Harbin Institute of Technology (HIT), Harbin, China, 2015, he is currently pursuing the Ph.D. degree in electrical engineering.

His research interests include linear motor drive and control, predictive current control, adaptive control, and sliding mode control.

MING-YI WANG was born in Jilin, China. He received the B.E., M.E., and Ph.D. degrees in electrical engineering from the Harbin Institute of Technology (HIT), Harbin, China, in 2009, 2011, and 2016, respectively.

He is currently with the Institute of Electromagnetic and Electronic Technology, HIT. His research interests include motor drive control, power electronic applications, and magnetic levitation.

LI-YI LI (M'09) received the B.E., M.E., and D.E. degrees from the Harbin Institute of Technology (HIT), Harbin, China, in 1991, 1995, and 2001, respectively. Since 2004, he has been a Professor with the School of Electrical Engineering and Automation, HIT.

In 2013, he became the Yangtze Fund Scholar Distinguished Professor. He is currently supported by the National Science Fund for Distinguished Young Scholars. He has authored or co-authored over 110 technical papers. He holds 50 patents. His research interests include design, drive, and control of linear motors and design and drive of high-speed/power density permanent magnet machines.

CHENG-MING ZHANG received the B.E., M.E., and D.E. degrees from the Harbin Institute of Technology (HIT), China, in 2005, 2007, and 2013, respectively. Since 2013, he has been a Lecturer with the School of Electrical Engineering and Automation, HIT.

His research interests include design and drive of linear motors, high-efficiency motor systems, and energy conversion and control.

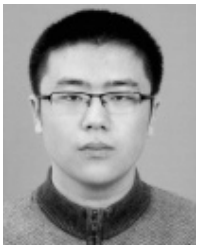

JIA-LIN JIANG was born in Jiamusi, China. He received B.E. degree in electrical engineering from the Harbin Institute of Technology (HIT), Harbin, China, in 2017, where he is currently pursuing the M.E. degree in electrical engineering.

His research interests include linear motor drive and control, and sliding mode control.